buildings

MDPI

*Article*

# Impact of Inorganic Salts on Rheology, Strength, and Microstructure of Excess-Sulfate Phosphogypsum Slag Cement

**Zhe Chen [1], Zixin Xue [1], Yong Xia [1], Chunli Wu [1], Junming Mai [1], Weisen Liu [2], Yuan Feng [2,*] and Jianhe Xie [2,3]**

[1] Guangdong Building Materials Institute Co., Ltd., Guangzhou 511455, China; dy314159@163.com (Z.C.); xuezixin717@163.com (Z.X.); cxiayong@163.com (Y.X.); c1028217763@163.com (C.W.); popinmai@126.com (J.M.)
[2] School of Civil and Transportation Engineering, Guangdong University of Technology, Guangzhou 510006, China; 1112209005@mail2.gdut.edu.cn (W.L.); jhxie@gdut.edu.cn (J.X.)
[3] Guangdong AIB Polytechnic, Guangzhou 510507, China
* Correspondence: fengyuan@gdut.edu.cn

**Abstract**

Excess-sulfate phosphogypsum slag cement (EPSC), offering the potential for large-scale phosphogypsum (PG) utilization, has drawn significant attention. However, its susceptibility to salt erosion in marine/saline environments remains unquantified, hindering engineering applications. This study, therefore, systematically investigates the effect of various salts (NaCl, $MgCl_2$, KCl, and $Na_2SO_4$) at different concentrations (0.5–1.5%) on the hydration mechanism and performance of EPSC using rheometry, strength tests, and microstructural characterization (XRD/SEM-EDS). The findings reveal that EPSC exhibits low initial yield stress and plastic viscosity, both of which increase over time. The addition of $Na^+$, $Cl^-$, and $SO_4^{2-}$ ions promotes hydration and flocculent structure formation in the EPSC paste, thereby enhancing the yield stress and plastic viscosity. In contrast, $Mg^{2+}$ and $K^+$ ions inhibit the hydration reaction, although $Mg^{2+}$ temporarily increases the plastic viscosity by forming $Mg(OH)_2$ during the initial stage of the reaction. Both $Na_2SO_4$ and NaCl improve mechanical properties when their concentrations are within the 0.5–1.0% range; however, excessive amounts (>1%) negatively impact these properties. Significantly, adding 0.5% NaCl significantly improves the mechanical properties of EPSC, achieving a 28-day compressive strength of 51.06 MPa—a 9.5% increase compared to the control group. XRD and SEM-EDX analyses reveal that NaCl enhances pore structure via Friedel's salt formation, while $Na_2SO_4$ promotes the early nucleation of ettringite. However, excessive ettringite formation in the later stages of the hydration reaction due to $Na_2SO_4$ may negatively affect compressive strength due to the inherent abundance of $SO_4^{2-}$ in the EPSC system. Therefore, attention should be paid to the effect of excessive $SO_4^{2-}$ on the system. These results establish salt-type/dosage thresholds for EPSC design, enabling its rational use in coastal infrastructure where salt resistance is critical.

**Keywords:** excess-sulfate phosphogypsum slag cement (EPSC); inorganic salts; rheological behavior; mechanical properties; microstructure

check for updates

Academic Editor: Mauro Mitsuuchi Tashima

Received: 10 June 2025
Revised: 27 June 2025
Accepted: 2 July 2025
Published: 4 July 2025

**Citation:** Chen, Z.; Xue, Z.; Xia, Y.; Wu, C.; Mai, J.; Liu, W.; Feng, Y.; Xie, J. Impact of Inorganic Salts on Rheology, Strength, and Microstructure of Excess-Sulfate Phosphogypsum Slag Cement. *Buildings* **2025**, *15*, 2348. https://doi.org/10.3390/buildings15132348

**Copyright:** © 2025 by the authors. Licensee MDPI, Basel, Switzerland. This article is an open access article distributed under the terms and conditions of the Creative Commons Attribution (CC BY) license (https://creativecommons.org/licenses/by/4.0/).

## 1. Introduction

Portland cement is the world's most widely used cementitious material and has been a cornerstone of modern infrastructure development. However, producing it requires a substantial amount of limestone and fuel. This contributes approximately 8% to global $CO_2$ emissions and releases pollutants such as dust and nitrogen oxides. Portland cement

is the most widely used cementitious material in the world and has been a cornerstone of modern infrastructure development [1]. China's cement output reached 2.35 billion tons in 2019 alone, exacerbating severe environmental problems [2]. Consequently, developing new binder materials that emit fewer carbon emissions and can utilize more solid waste has become a critical focus in the field of building materials [3–5].

Conversely, the production scale of phosphoric acid and phosphate fertilizers continues to expand alongside the rapid advancement of global industrialization. Phosphogypsum (PG), a by-product of the wet-process phosphoric acid industry, has seen a dramatic increase in annual output. For every ton of phosphoric acid produced, approximately five tons of PG are generated, resulting in global annual emissions of over 300 million tons. However, the comprehensive utilization rate of PG remains alarmingly low at under 15% [6]. The primary component of PG is calcium sulfate dihydrate ($CaSO_4 \cdot 2H_2O$), which is often contaminated with fluoride, phosphate, and heavy metals (such as Cr, As, Ba, Zn, etc.). Some PG even contains radioactive elements, and when stored in the open air, it is prone to causing soil pollution and radioactive diffusion issues [7,8]. Under the dual pressures of stricter environmental governance and economic transformation, the resource utilization technology of PG has become a research hotspot. In the agricultural field, PG is utilized as a soil amendment [9]. However, this practice poses risks, such as heavy metals infiltrating the food chain. In the building materials industry, PG can be used as an alternative to natural gypsum in the production of retarders or low-strength gypsum products. Nevertheless, soluble impurities in PG can significantly increase setting times and reduce early strength [10]. When used as a cement admixture or aggregate, adding more than 10% PG can reduce 28-day compressive strength by 15–30%. However, in recent years, research has demonstrated that $Ca^{2+}$ and $SO_4^{2-}$ positively contribute to geopolymer reactions, prompting increased attention toward the potential application of PG in geopolymer materials [11,12]. However, this approach encounters challenges such as high costs and safety concerns. Strong alkaline activators (such as NaOH and $Na_2SiO_3$) are expensive (accounting for about 60% of the total material cost) [13,14], while the use of high pH pastes raises significant safety risks during construction. Overall, the resource utilization technology of PG is hindered by the dual challenges of "low solid waste disposal efficiency" and "limited product added value".

Excess-sulfate phosphogypsum slag cement (EPSC) has received a lot of attention because of its potential to enable the large-scale utilization of PG [15]. EPSC is primarily composed of industrial solid waste, typically consisting of 45–55% ground granulated blast furnace slag (GGBFS), 45% PG, and around 5% Portland cement (used as an alkali activator) [16]. Its production process eliminates the need for calcination and incorporates minimal clinker, thereby reducing both energy consumption and $CO_2$ emissions [17]. Furthermore, EPSC has been demonstrated to effectively immobilize harmful heavy metals and soluble phosphorus impurities [18]. EPSC offers a new approach to the large-scale, high-value utilization of PG that is more aligned with the concept of sustainable, green building materials. Research indicates that the hydration products of EPSC are primarily C-(A)-S-H gel and ettringite, achieving a compressive strength of 40–60 MPa after 28 days. Most studies have focused on optimizing the proportions of EPSC. For example, using steel slag as an alkali activator has been shown to significantly improve performance at an early stage, achieving a compressive strength of 28 MPa within 7 days [16]. Tao et al. [17] explored the feasibility of using calcium sulfoaluminate cement as an alkaline activator. Zhang et al. [19] optimized the setting time of EPSC using a Paste Rheological Threshold theory. However, as a cementitious material derived from solid waste, its potential engineering applications (such as coastal dams and subgrades in saline soil areas) generally face the risk of erosion due to high salt concentrations ($Cl^-$, $SO_4^{2-}$, $Mg^{2+}$, etc.). A lack of systematic understanding

remains of the effects of such salts, guaranteeing that the long-term service performance of EPSC, including its impermeability and volume stability, remains a critical challenge.

Scholars have extensively investigated the influence of salts on the properties of traditional Portland cement and geopolymers, with the aim of optimizing their performance in coastal and erosive environments [20,21]. Salt ions often have a dual effect on these materials. In the short term, $Cl^-$ promotes pore densification by forming Friedel's salts; however, over time, this can increase the risk of steel corrosion [22,23]. Under alkaline conditions, $SO_4^{2-}$ reacts with aluminates to form ettringite, strengthening the interfacial transition zone in the early stages. However, an excessive concentration of $SO_4^{2-}$ can cause expansion and cracking. This issue is particularly significant in geopolymers, as calcium-containing precursors (such as GGBFS) can produce gypsum ($CaSO_4 \cdot 2H_2O$) and ettringite in an $SO_4^{2-}$ environment. This leads to expansion stress, with a volume expansion rate of >0.1% causing microcracks [24]. Additionally, $Mg^{2+}$ replaces $Ca^{2+}$ in C-S-H, forming the weaker, lower-strength compound $Mg(OH)_2$ and reducing the alkalinity and stability of the binder phase [25]. These findings demonstrate that the performance of binders, including traditional Portland cement and geopolymers, is influenced by salts through mechanisms such as ion exchange and the formation of expansive phases.

In EPSC, the high sulfate content and system richness in ettringite may exacerbate sensitivity to salt erosion. Additionally, impurities in PG, such as $PO_4^{3-}$, may alter the reaction pathways of salts. External salts can disrupt the efficiency of sulfate activation or modify hydration mechanisms via ion competition; for example, $Cl^-$ inhibits ettringite formation. EPSC utilizes PG as its source of sulfate activation, with the hydration products primarily consisting of ettringite and C-(A)-S-H gel, which is a significant departure from traditional cement and geopolymers [15–17]. The presence of external salts, such as $SO_4^{2-}$ in seawater, can induce ion migration driven by concentration gradients. This can trigger secondary ettringite crystallization, increasing the risk of expansion damage. There is a competitive interplay between $Cl^-$ and $SO_4^{2-}$, whereby $Cl^-$ may preferentially bind with aluminum to form Friedel's salt, thereby depleting the $Al^{3+}$ necessary for ettringite production. Research suggests that ettringite is unstable in chloride-rich environments and may facilitate the formation of Friedel's salt in cement paste containing $Cl^-$ [26], and ettringite may help form Friedel's salt in cement paste containing chloride ions [26]. Furthermore, $Mg^{2+}$ can compromise the primary strength phase of EPSC by replacing $Ca^{2+}$ in the C-(A)-S-H gel through a substitution reaction, thereby diminishing structural integrity. Despite ongoing research, the effects of various salt types and concentrations on the mechanical properties and microstructure of EPSC remain insufficiently understood. This knowledge gap significantly limits its application in critical scenarios, such as marine engineering. Another challenge facing EPSC is its insufficient early strength. It remains unclear whether the addition of salts, which has proven beneficial in enhancing early strength for cement-based materials and geopolymers, could yield similar improvements in EPSC [21]. Addressing these uncertainties is essential for advancing EPSC's practical implementation.

In the alkali-activated GGBFS reaction system, the concentration of $OH^-$ ions plays a pivotal role in the hydration process of GGBFS, directly influencing the characteristics of its hydration products [27–29]. Research by Song et al. [27] shows that effective hydration of GGBFS necessitates maintaining a pH value above 11.5. When the pH drops below 9.5, the hydration process ceases entirely. A higher pH value not only significantly enhances the efficiency of the GGBFS hydration reaction but also accelerates setting time and improves the resulting mechanical properties. Consequently, investigating the impact of various salts on the pH value of freshly mixed EPSC paste is of substantial research significance.

In this study, EPSCs were developed by combining PG, GGBFS, and cement. To assess the influence of various salt types and contents on EPSC, the research examined

the effects of different salt (NaCl, $MgCl_2$, KCl, and $Na_2SO_4$) contents on the rheological and mechanical properties (compressive strength and flexural strength). Furthermore, the properties and microstructure of both the raw materials and the EPSC were analyzed using X-ray diffraction (XRD) and scanning electron microscopy (SEM) combined with energy-dispersive X-ray spectroscopy (EDX). The objective of this study is to deepen the understanding of how different salts and their contents impact the performance of EPSC.

## 2. Materials and Methods

### *2.1. Raw Materials*

The raw materials utilized in this study comprise PG, GGBFS, and ordinary Portland cement, as shown in Figure 1. PG, sourced from Yunnan Province, presents a gray appearance, while GGBFS is a fine white powder. Ordinary Portland cement is supplied by Fushun Cement Co., Ltd., Fushun, Liaoning, China. The chemical compositions of the raw materials, determined by XRF, are detailed in Table 1. From a chemical composition perspective, PG primarily consists of CaO and $SO_3$, whereas GGBFS is rich in the three major components of CaO, $SiO_2$, and $Al_2O_3$. Their mineralogical phases were identified by XRD analysis (Figure 2). The primary components of PG include $CaSO_4 \cdot 2H_2O$ and $CaSO_4 \cdot 0.5H_2O$, with detectable $P_2O_5$ impurities (1.2%). These impurities, consisting of soluble phosphorus and eutectic phosphorus, significantly impede the hydration process of EPSC by releasing interfering ions. XRD analysis reveals a distinct amorphous phase in GGBFS within the 20–40° range, as depicted in Figure 2b. Within the EPSC system, GGBFS reacts with PG and the $Ca(OH)_2$ produced by cement hydration to form the primary hydration products, C-(A)-S-H gel and ettringite [30–32].




**Figure 1.** Photographs of EPSC raw materials: (**a**) PG, (**b**) GGBFS, and (**c**) cement.

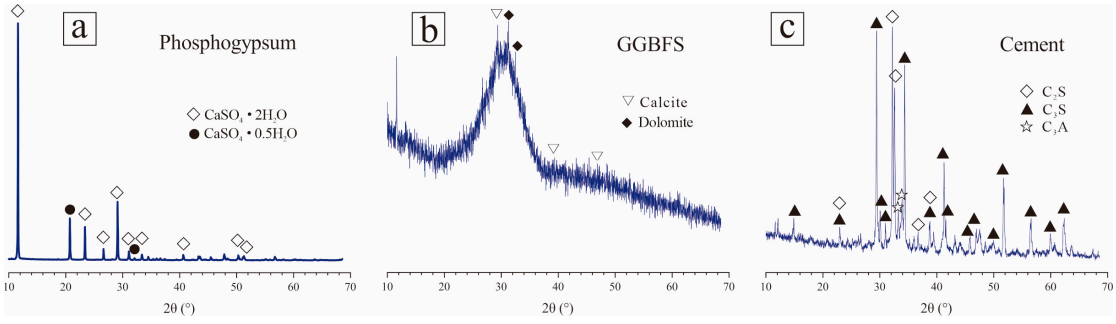


**Figure 2.** XRD patterns of EPSC raw materials: (**a**) PG, (**b**) GGBFS, and (**c**) cement.

In addition, NaCl, $MgCl_2$, KCl, and $Na_2SO_4$ (with a purity of ≥96%) were utilized as additive salts. All chemical agents were sourced from commercial suppliers.

**Table 1.** Chemical composition of EPSC raw materials (wt.%).

| Raw Material | CaO | $SiO_2$ | $Al_2O_3$ | $Fe_2O_3$ | $SO_3$ | MgO | $Na_2O$ | $P_2O_5$ | Others |
|---|---|---|---|---|---|---|---|---|---|
| Phosphogypsum | 42.9 | 3.8 | 0.5 | 0.4 | 50.5 | 0.4 | 0.04 | 1.2 | 0.3 |
| GGBFS | 42.7 | 29.6 | 13.7 | 0.6 | 2.9 | 0.6 | 7.3 | 0.02 | 2.6 |
| Cement | 76.2 | 11.5 | 2.5 | 3.9 | 3.8 | / | / | / | 2.1 |

### *2.2. Mixture Design and Preparation Methods*

#### 2.2.1. Pretreatment of EPSC Raw Materials

The industrial by-product PG often absorbs a certain amount of moisture during the emission process. Prolonged open storage can lead to caking. In addition, the soluble phosphate and fluoride ions in PG not only cause the EPSC paste to exhibit acidity but also react with $Ca^{2+}$ to form $Ca_5(PO_4)_3OH$ and $CaF_2$ precipitates, resulting in a dual inhibition of the alkaline activation reaction of GGBFS. By removing these impurities through water washing pretreatment, the release of $Ca^{2+}$ / $Al^{3+}$ from slag can be significantly promoted, thereby optimizing the formation of ettringite and C-(A)-S-H gel. Therefore, PG pretreatment is a critical step in enhancing the performance of EPSC.

The processing steps are outlined as follows: First, PG undergoes a water washing treatment and is subsequently dried at 40 °C for 48 h. This washing process effectively removes soluble phosphorus and fluorine impurities from the PG. Following the water washing, the PG is mixed with deionized water at a mass ratio of 1:10 and soaked for 1 h. The pH value of the suspension is measured to be 6.8, confirming that the water washing treatment significantly mitigates PG's adverse effects on the setting time of EPSC. Next, the PG is mixed with GGBFS at a mass ratio of 1:1, and ground in a grinder at a speed of 48 r/min for 5 min. This process culminates in the preparation of the EPSC raw materials.

The particle size distribution of the raw materials was determined using a Mastersizer 3000 laser particle size analyzer (Malvern, Britain) (Figure 3a,b). The $D_{50}$ particle sizes of PG, GGBFS, and EPSC were 20.3 μm, 10.3 μm, and 23.7 μm, respectively. The SEM image of PG (Figure 3c) revealed rhombic, plate-like particles with a rough surface. However, following grinding, fully intact rhombic, plate-like PG particles were absent in the resulting EPSC raw material (Figure 3e). This enhanced the dissolution of $Ca^{2+}$/$SO_4^{2-}$ ions, promoting ettringite nucleation.

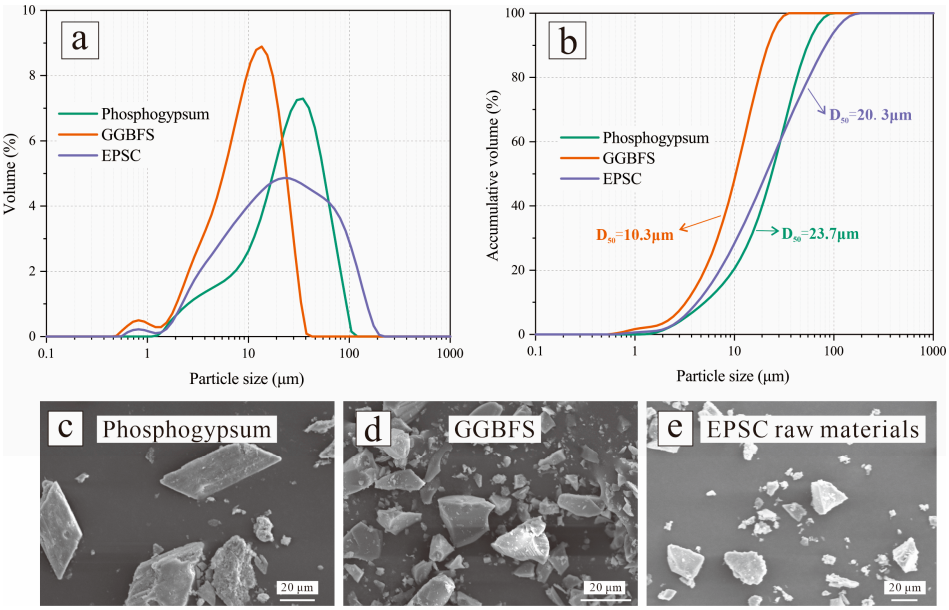


**Figure 3.** Particle size distributions and SEM of raw materials: (**a**,**b**) particle size distributions of PG, GGBFS, and EPSC, and SEM of (**c**) PG, (**d**) GGBFS, and (**e**) EPSC raw materials.

2.2.2. Preparation of EPSC with Addition of Salts

The content of salts (NaCl, KCl, $MgCl_2$, $Na_2SO_4$) as a percentage of the total mass of raw materials was set at 0.5 wt%, 1.0 wt%, and 1.5 wt% (Figure 4). These salts were separately dissolved with distilled water to prepare individual solutions. Each salt solution was then thoroughly mixed with the EPSC raw material and cement for 2 min to form a homogeneous paste. This uniform paste was poured into plastic prism molds measuring 40 mm × 40 mm × 160 mm and compacted using a vibrator for 60 s to eliminate air bubbles. The specimens were subsequently cured in a humid environment at a temperature of 20 ± 2 °C and a relative humidity of 95 ± 5%. After 7 days, the EPSC specimens were demolded and stored in a humid environment until their mechanical properties, including flexural and compressive strength, were fully developed for testing at 7 and 28 days. The resulting products were labeled as "X-Y," where "X" denoted the type of salt, and "Y" represented the salt content. For instance, "NaCl-0.5" referred to EPSC containing 0.5 wt% NaCl. Following the raw material composition of previously developed EPSCs, the proportions of PG and GGBFS in this study were maintained at 50% each, with an additional 4% of Portland cement used as an alkali activator. Distilled water was employed as the mixing water, and the specific EPSC mix proportions are outlined in Table 2.

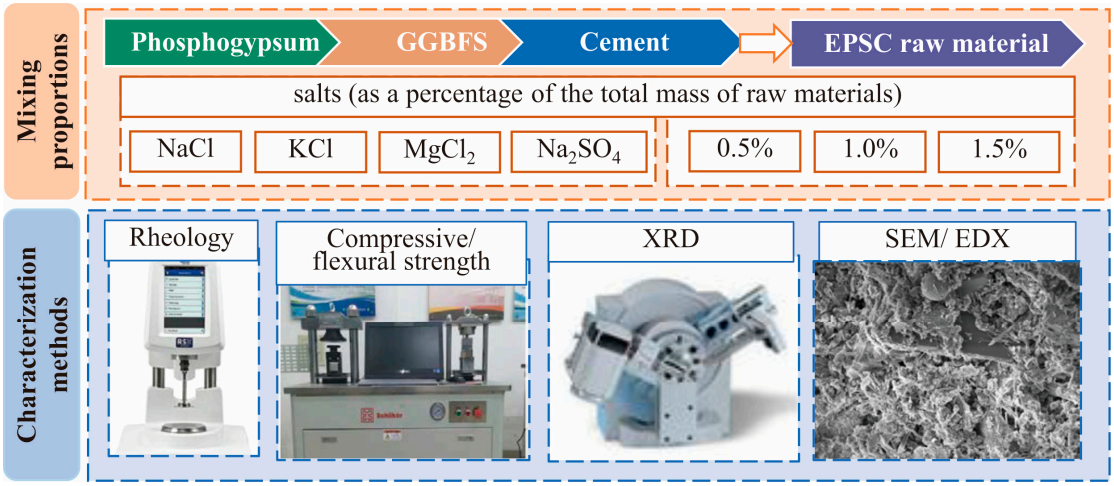


**Figure 4.** Methodological framework.

**Table 2.** Mixing proportions of EPSCs (kg/m$^3$).

| No. | Salt Type | Dosage (%) |
|---|---|---|
| Ref. | / | |
| NaCl-0.5% | NaCl | 0.5 |
| NaCl-1.0% | NaCl | 1.0 |
| NaCl-1.5% | NaCl | 1.5 |
| KCl-0.5% | KCl | 0.5 |
| KCl-1.0% | KCl | 1.0 |
| KCl-1.5% | KCl | 1.5 |
| $MgCl_2$-0.5% | $MgCl_2$ | 0.5 |
| $MgCl_2$-1.0% | $MgCl_2$ | 1.0 |
| $MgCl_2$-1.5% | $MgCl_2$ | 1.5 |
| $Na_2SO_4$-0.5% | $Na_2SO_4$ | 0.5 |
| $Na_2SO_4$-1.0% | $Na_2SO_4$ | 1.0 |
| $Na_2SO_4$-1.5% | $Na_2SO_4$ | 1.5 |

Note: Fixed parameters: PG = 1000 kg/m$^3$, GGBFS = 0 kg/m$^3$, cement = 0 kg/m$^3$, distilled water = 1000 kg/m$^3$.

### 2.3. Characterization Methods

The pH value of the freshly prepared EPSC paste was measured using a Shanghai Leici PHS-3C pH meter (Shanghai Yidian Scientific Instrument Co., Ltd., Shanghai, China). The specific method involved weighing 1 g of the freshly mixed paste, adding 10 g of distilled water, thoroughly mixing the solution for 1 h, and then performing a precise measurement using the pH meter.

This study utilized the RSX coaxial rotational rheometer to evaluate the rheological properties of EPSC. Prior to formal testing, the EPSC paste underwent a pre-shearing process at a constant shear rate of 100 $s^{-1}$ for 80 s, followed by a 60 s rest period to ensure uniformity across all samples and establish a consistent initial state. During the formal testing phase, the shear rate was progressively increased from 0 $s^{-1}$ to 100 $s^{-1}$ within 0–60 s, then gradually decreased from 100 $s^{-1}$ to 0 $s^{-1}$ over the next 60 s, completing the entire testing cycle. The rheological loading mechanism of EPSC throughout the testing process is depicted in Figure 5.

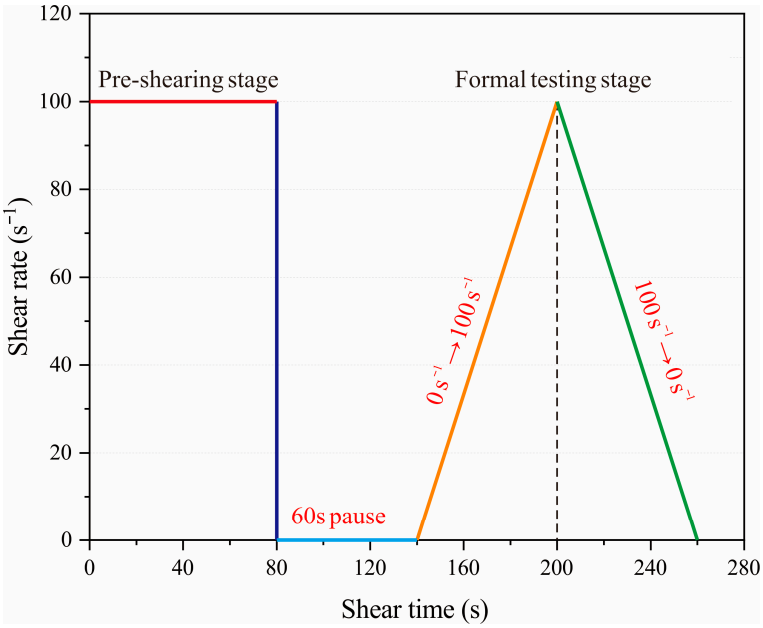


**Figure 5.** Schematic of the rheological loading protocol of EPSC paste.

The compressive and flexural strength tests were conducted in accordance with the GB/T 17671-2021 standard [33]. Mortar was mixed using a cement-to-sand ratio of 1:3, and standard test specimens with dimensions of 40 mm × 40 mm × 160 mm were prepared. The tests were conducted following curing periods of 7 days and 28 days. During the flexural strength test, the loading rate was maintained within a range of 50 ± 10 N/s. After the test was completed, the fractured specimen was placed in the compressive testing machine, where the compressive strength test was conducted at a loading rate of 2400 ± 200 N/s.

Phase analysis of the raw materials and EPSC samples was conducted using a Bruker D8 Advance X-ray diffractometer (Mannheim, Germany). The experimental parameters included a CuKα radiation source, operating at a voltage of 40 kV and a current of 40 mA. Measurements were conducted within a 2θ range of 10° to 70°, with a scanning speed of 5° per minute. The resulting XRD patterns were processed and analyzed using MDI Jade 9 software.

SEM imaging coupled with energy-dispersive X-ray spectroscopy (SEM-EDX) was obtained using a TESCAN MIRA LMS scanning electron microscope (Tescan Co., Ltd., Brno, Czech) to observe and analyze the changes in the microstructure and elemental

composition of EPSC after adding different salts. Prior to testing, the samples were dried and treated with a Au layer, and the accelerating voltage was set at 15 kV.

## 3. Results and Discussions

### *3.1. pH Value*

As illustrated in Figure 6, the addition of NaCl, $MgCl_2$, and KCl had a negligible effect on the pH value of the paste, which remained consistently stable within the range of 11.28 to 11.34. In contrast, the incorporation of $Na_2SO_4$ exerted a notable impact: as the concentration of $Na_2SO_4$ increased, the pH value of the paste demonstrated an upward trend. For example, the addition of just 0.5% $Na_2SO_4$ raised the pH value of the slurry from 11.31 to 11.71, significantly promoting the hydration reaction of GGBFS. This effect arises from the chemical interaction between $Na_2SO_4$ and $Ca(OH)_2$, which produces NaOH and $CaSO_4$. The resulting increase in the pH of the solution accelerates the hydration reaction of GGBFS [34].

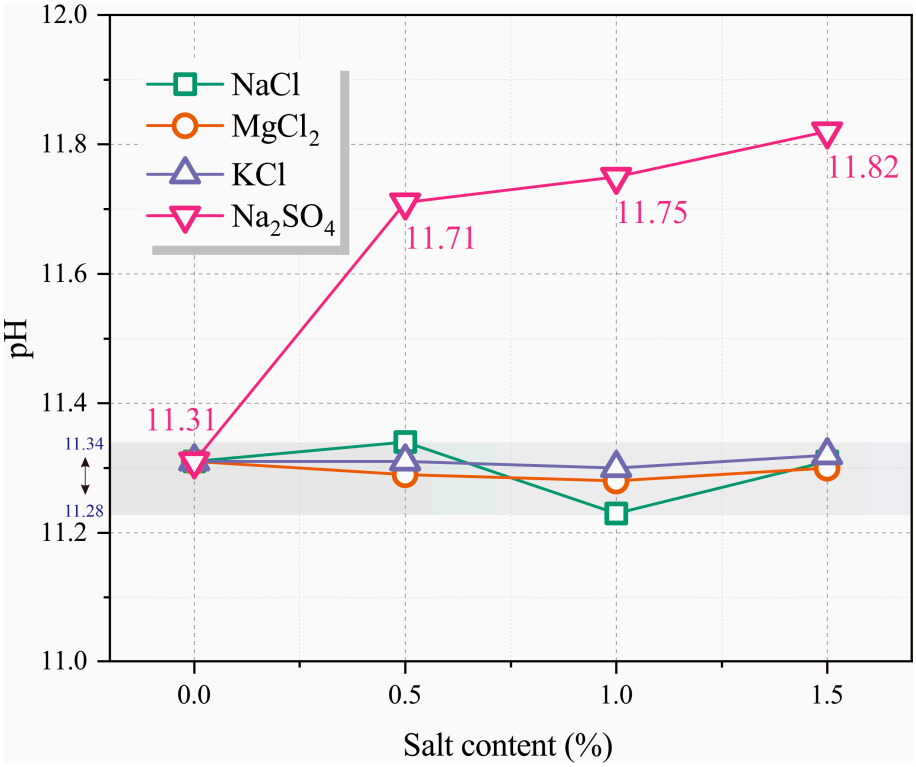


**Figure 6.** Effect of salt content on the pH levels of EPSC paste.

### *3.2. Rheological Properties*

To assess the impact of various factors on the rheological properties of EPSC, the modified Bingham model [35] was chosen to analyze the experimental data. The mathematical representation of the modified Bingham model is presented in Equation (1):

$$\tau = \tau_0 + \eta\gamma + c\gamma^2 \quad (1)$$

where $\tau$ denotes the shear stress, $\tau_0$ represents the yield stress, $\eta$ signifies the plastic viscosity, $\gamma$ refers to the shear rate, and $c$ characterizes the extent of deviation from linearity in the fluid's rheological properties. A positive value of $c$ ($c > 0$) indicates shear thickening, while a negative value ($c < 0$) signifies shear thinning. When $c$ equals zero ($c = 0$), the system conforms to the Bingham model.

The modified Bingham model was prioritized over Bingham model (linear assumption) and Herschel–Bulkley model (extra power-law parameter) alternatives for dual reasons: (1) It accurately characterizes the nonlinear flow of flocculated EPSC paste (see $c < 0$ in Table 3) with minimal complexity. (2) It achieves superior fitting ($R^2 > 0.98$ universally) for such low-variance systems.

**Table 3.** The rheological fitting curve of EPSC under varying factors.

| No. | Time (min) | $\tau_0$ | $\eta$ | $c$ | $R^2$ |
|---|---|---|---|---|---|
| Without salts | 0 | 28.14 | 0.045 | 0.003 | 0.99 |
| | 5 | 28.80 | 0.065 | 0.003 | 0.99 |
| | 10 | 29.46 | 0.075 | 0.003 | 0.99 |
| | 15 | 29.98 | 0.081 | 0.003 | 0.99 |
| | 20 | 30.35 | 0.091 | 0.003 | 0.99 |
| | 25 | 30.66 | 0.105 | 0.003 | 0.99 |
| | 30 | 30.83 | 0.114 | 0.003 | 0.99 |
| NaCl-1.0% | 0 | 29.34 | 0.076 | 0.003 | 0.99 |
| | 5 | 29.89 | 0.104 | 0.003 | 0.99 |
| | 10 | 30.31 | 0.115 | 0.003 | 0.99 |
| | 15 | 30.59 | 0.126 | 0.003 | 0.99 |
| | 20 | 30.95 | 0.134 | 0.003 | 0.99 |
| | 25 | 31.27 | 0.139 | 0.002 | 0.99 |
| | 30 | 31.32 | 0.151 | 0.002 | 0.99 |
| KCl-1.0% | 0 | 29.03 | 0.077 | 0.003 | 0.99 |
| | 5 | 26.93 | 0.081 | 0.003 | 0.99 |
| | 10 | 25.64 | 0.083 | 0.003 | 0.99 |
| | 15 | 24.94 | 0.086 | 0.003 | 0.99 |
| | 20 | 24.45 | 0.087 | 0.003 | 0.99 |
| | 25 | 24.14 | 0.085 | 0.003 | 0.99 |
| | 30 | 23.91 | 0.087 | 0.003 | 0.99 |
| $MgCl_2$-1.0% | 0 | 26.59 | 0.024 | 0.003 | 0.99 |
| | 5 | 25.81 | 0.033 | 0.003 | 0.99 |
| | 10 | 25.62 | 0.031 | 0.003 | 0.99 |
| | 15 | 25.29 | 0.048 | 0.003 | 0.99 |
| | 20 | 25.51 | 0.036 | 0.003 | 0.99 |
| | 25 | 25.28 | 0.046 | 0.003 | 0.99 |
| | 30 | 25.35 | 0.044 | 0.003 | 0.99 |
| $Na_2SO_4$-1.0% | 0 | 31.48 | 0.120 | 0.003 | 0.99 |
| | 5 | 32.13 | 0.141 | 0.002 | 0.99 |
| | 10 | 32.49 | 0.161 | 0.002 | 0.99 |
| | 15 | 32.88 | 0.177 | 0.002 | 0.99 |
| | 20 | 33.12 | 0.191 | 0.002 | 0.99 |
| | 25 | 33.40 | 0.199 | 0.002 | 0.99 |
| | 30 | 33.62 | 0.208 | 0.002 | 0.99 |

Through curve fitting, the relationship between shear rate and shear stress was derived (Figure 7a), and the corresponding rheological equations and models are presented in Table 3. As illustrated in Figure 7a, the rheological fitting curves of EPSCs from various groups display nonlinear variations. The rheological properties of EPSCs were analyzed using the modified Bingham model, yielding an $R^2$ value exceeding 0.98. This high $R^2$ value demonstrates that the modified Bingham model effectively captures and describes the rheological characteristics of the EPSCs in this study.

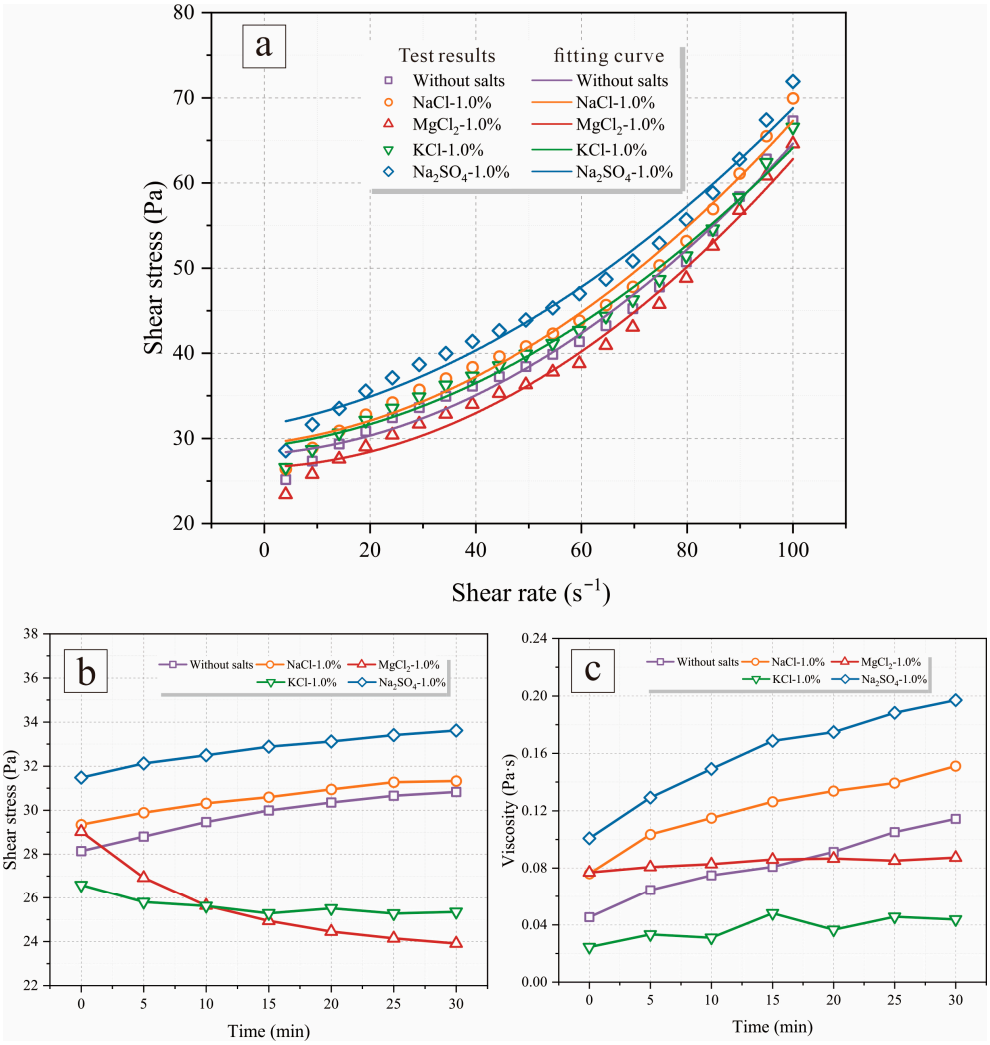


**Figure 7.** Rheological properties of EPSCs: (**a**) shear stress as a function of shear rate, (**b**) shear stress as a function of time, and (**c**) viscosity as a function of time.

The initial (0 min) plastic viscosity of EPSC is lower than that of cement paste with a comparable water/binder ratio [36], measuring only 0.045 Pa·s in the absence of added salt. This remarkably low viscosity can be primarily attributed to two key factors. First, the principal component of PG, $CaSO_4 \cdot H_2O$, lacks cementitious properties. Although it occupies the solid phase volume, it does not contribute to bonding forces, and its layered structure likely enhances lubrication, further reducing viscosity. Second, GGBFS requires an alkaline environment to activate its reactivity. However, during the initial stage of the hydration reaction, the limited amount of $Ca(OH)_2$ (4%) released by Portland cement results in a slow hydration process.

Upon the addition of NaCl, $MgCl_2$, and $Na_2SO_4$, a noticeable increase in the initial plastic viscosity and yield stress of EPSC was observed, with the most pronounced effect occurring when 1% $Na_2SO_4$ was added. $Na^+$ and $Cl^-$ ions reduce electrostatic repulsion between particles by compressing the electric double layer, which facilitates the formation of flocculent structures. Furthermore, $Cl^-$ reacts with $Al_2O_3$ in GGBFS to form Friedel's salt, while $SO_4^{2-}$ reacts with $Al_2O_3$ in slag to produce ettringite. These reactions greatly enhance structural integrity, thereby increasing both the yield stress and plastic viscosity of the slurry. Owing to its high reactivity, $Na_2SO_4$ significantly accelerates the hydration process of EPSC raw materials.

The introduction of $Mg^{2+}$ can lead to the formation of $Mg(OH)_2$, which temporarily increases viscosity by filling pores. Furthermore, compared to $Na^+$, $K^+$ possesses a larger ionic radius, making it less effective in compressing the electric double layer. This can result in inadequate flocculation and hinder hydration reactions, ultimately reducing both yield stress and plastic viscosity.

The rheological properties of the EPSCs in each group were significantly affected by shear rate and time, which are intrinsically linked to the formation of flocculated gel [37]. In salt-free EPSCs, the hydration of Portland cement generates $Ca(OH)_2$, progressively increasing the pH of the liquid phase (>11, as discussed in Section 3.1). This elevated pH promotes the dissolution of the glassy phase in GGBFS, releasing ions such as $Ca^{2+}$, $Si^{4+}$, and $Al^{3+}$. These released ions gradually form C-(A)-S-H gel and ettringite, creating a cohesive network between particles and thereby increasing flow resistance. Consequently, both plastic viscosity and yield stress rise over time. However, as hydration progresses, the concentration of $Ca^{2+}$ and $OH^-$ in the liquid phase decreases, and the resistance to ion migration intensifies. This results in a deceleration of the hydration rate, leading to a corresponding slowdown in the increase of plastic viscosity.

After the addition of 1% NaCl and $Na_2SO_4$, the plastic viscosity and yield stress increased significantly, indicating that these two salts accelerated the hydration reaction of EPSC, resulting in the formation of more hydration products within the first 30 min. Notably, the introduction of $MgCl_2$ also led to an initial increase in both yield stress and plastic viscosity. However, over time, the yield stress gradually decreased while the plastic viscosity remained constant. This behavior may be attributed to the encapsulation of $Mg(OH)_2$ in a colloidal state on the surface of cement particles, which forms a physical barrier and simultaneously lowers the system's pH. These conditions hinder the progression of the hydration reaction, limiting the early formation of C-(A)-S-H gel and ettringite, thereby weakening the bond strength between particles. After adding KCl, both the yield stress and plastic viscosity of EPSC decreased. It is worth noting that within the specified experimental time range, both rheological parameters remained relatively stable, with no significant time-dependent changes observed.

### *3.3. Flexural Strength and Compressive Strength*

Figure 8 illustrates the impact of different salt types and their concentrations on the 7 days and 28 days flexural strength of EPSC. The results reveal that variations in KCl concentration had a negligible effect on the flexural strength of EPSC. In contrast, the inclusion of NaCl, $MgCl_2$, and $Na_2SO_4$ followed a pattern of an initial increase in strength, followed by a decline. Specifically, when the concentrations of NaCl and $MgCl_2$ were 0.5%, the 28 days flexural strength of EPSC increased by 6.32% and 1.39%, respectively. For $Na_2SO_4$, the optimal concentration depended on the curing age: a 1% concentration was most effective at 7 days, while a 0.5% concentration yielded the best results at 28 days. Notably, a 0.5% concentration of $Na_2SO_4$ significantly enhanced the flexural strength of EPSC, achieving a 28 days flexural strength of 9.96 MPa—representing a 6.7% increase compared to the control group.

Figure 9 illustrates the impacts of different salt types and their concentrations on the compressive strength of EPSC at 7 days and 28 days. The findings reveal that the type of salt plays a critical role in influencing the compressive strength of EPSC. Regarding the 28 days compressive strength, the addition of $MgCl_2$ showed a relatively minimal effect. In contrast, for NaCl, KCl, and $Na_2SO_4$, an increase in their concentrations initially enhanced the compressive strength, followed by a subsequent decline. Notably, when the concentration of NaCl, KCl, and $Na_2SO_4$ reached 0.5%, the 28 days compressive strength of EPSC was maximized. Among these, NaCl exhibited the most significant effect, boosting

the 28 days compressive strength of EPSC to 51.06 MPa, representing a 9.5% increase. For $Na_2SO_4$, the optimal concentration depended on curing time: at 7 days, a 1% concentration was most effective, while at 28 days, a 0.5% concentration yielded the best results. It is important to note that when the concentration of $Na_2SO_4$ exceeds 1%, the compressive strength of EPSC begins to decline.

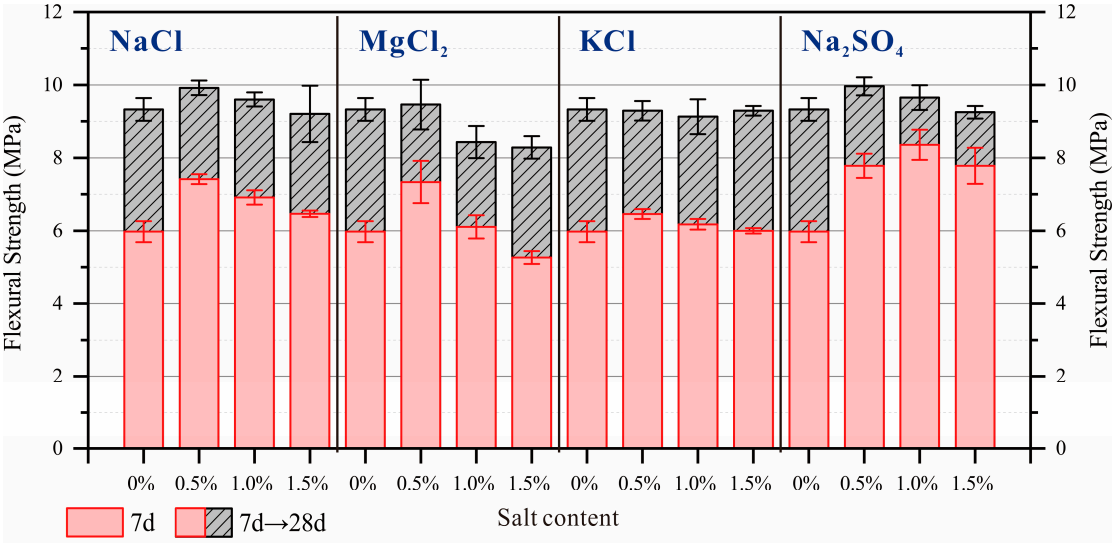


**Figure 8.** The effect of salt content on the flexural strength of EPSC.

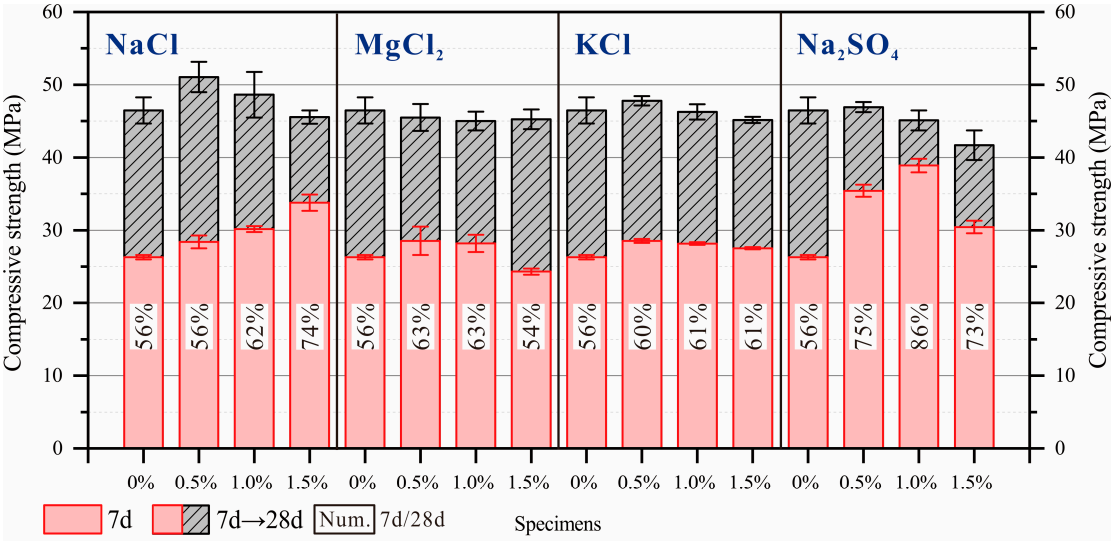


**Figure 9.** Effect of salt content on the compressive strength of EPSC.

Additionally, Figure 9 illustrates the ratio of 7 days compressive strength to 28 days compressive strength for each group of EPSCs. A higher ratio reflects better early-stage strength development in EPSCs. Without the addition of any salt, this ratio was 56%. As depicted in the figure, the inclusion of $MgCl_2$ and KCl slightly improved this ratio. In contrast, NaCl and $Na_2SO_4$ significantly enhanced the early-stage strength development of EPSCs, with the most notable improvement observed when 1% $Na_2SO_4$ was added. Under this condition, the 7 days compressive strength reached 86% of the 28 days compressive strength.

Previous studies on Portland cement have demonstrated that NaCl [38] and KCl [39] can accelerate hydration, likely due to the interaction between $Cl^-$ and aluminate phases. At lower doses, NaCl significantly enhances the hydration of Portland cement, while at higher doses, it retards the process [40]. Moreover, ion exchange reactions between $Na^+$

and $Ca^{2+}$ in the raw materials of EPSC—specifically GGBFS and PG—further promote the dissolution of calcium in GGBFS and PG [41].

Similarly, $Na_2SO_4$ has been shown to promote the early hydration rate of GGBFS [42]. The enhancement primarily depends on three key factors. First, as discussed in Section 3.1, the addition of $Na_2SO_4$ raises the pH value of the EPSC paste. This increase in pH accelerates the hydration of GGBFS, leading to the formation of a greater amount of hydrated gel and resulting in a denser matrix. Second, the presence of additional sulfate ions facilitates the formation of more AFt [43]. Studies have demonstrated that AFt-based cementitious materials exhibit higher early strength. Lastly, $Na_2SO_4$, being more soluble in water than PG, reacts with $Ca(OH)_2$ in the system to produce $CaSO_4$. This $CaSO_4$, characterized by higher dispersibility, is more reactive and more readily participates in the formation of AFt compared to PG [44]. However, the observed reduction in later strength development associated with the use of $Na_2SO_4$ is attributed to its effects on the microstructure, which will be analyzed further in Section 3.5.

In this study, the addition of NaCl demonstrated the most substantial enhancement in compressive strength among the EPSCs examined, whereas $Na_2SO_4$ proved to be the most effective in promoting early strength development.

Figure 10 illustrates the relationship between flexural strength and compressive strength in EPSCs across all groups. The experiment reveals that the addition of NaCl, $MgCl_2$, and KCl had a negligible effect on the flexural/compressive strength ratio of EPSCs; the ratio consistently remained within the range of 0.18 to 0.20. In contrast, the inclusion of $Na_2SO_4$ markedly improved the flexural/compressive strength ratio, significantly narrowing the gap between compressive strength and splitting strength. This improvement is likely attributed to the formation of needle-shaped ettringite crystals, whose distinct microstructure effectively bolsters the flexural performance of EPSCs.

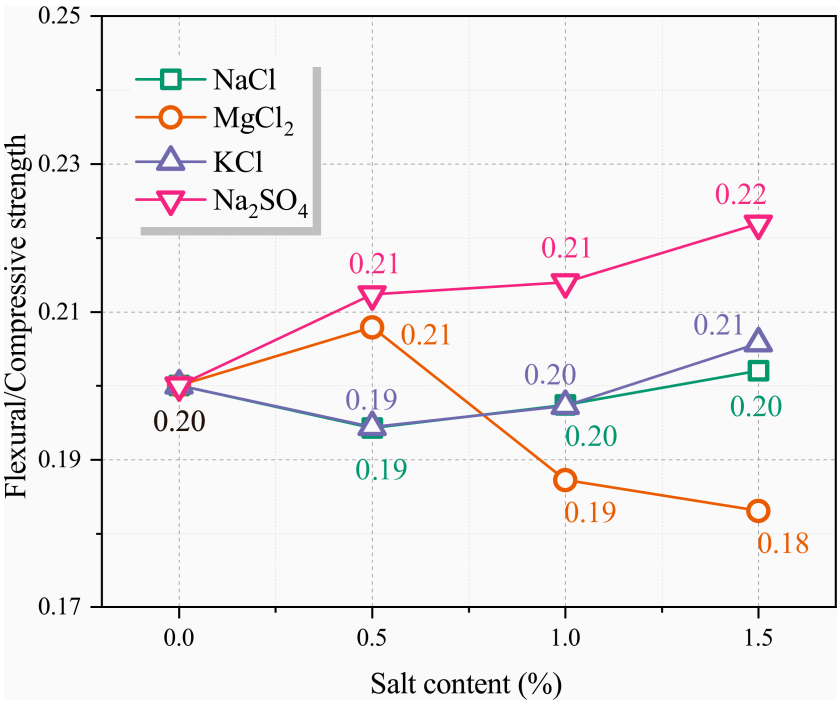


**Figure 10.** Flexural/compressive strength ratio of EPSCs.

### *3.4. XRD Patterns*

Figure 11 illustrates the comparative analysis of XRD patterns for EPSCs with and without added salt. In the case of EPSCs lacking salt, the predominant crystalline phases are dihydrate gypsum and ettringite. The gypsum phase originates both from the dihydrate

gypsum present in PG and the hydration process of hemihydrate gypsum, while ettringite forms during the later stages of hydration as a product of the ongoing reaction between the continuous hydration of GGBFS and gypsum under alkaline conditions [17,18]. A closer examination through local magnification (Figure 11b) reveals a distinct broad hump centered near 30° (2θ) in the XRD pattern of the EPSCs. Compared with the XRD pattern of GGBFS, this broad reflection peak is shifted to a higher angular region, indicating the formation of amorphous C-(A)-S-H gel [20].

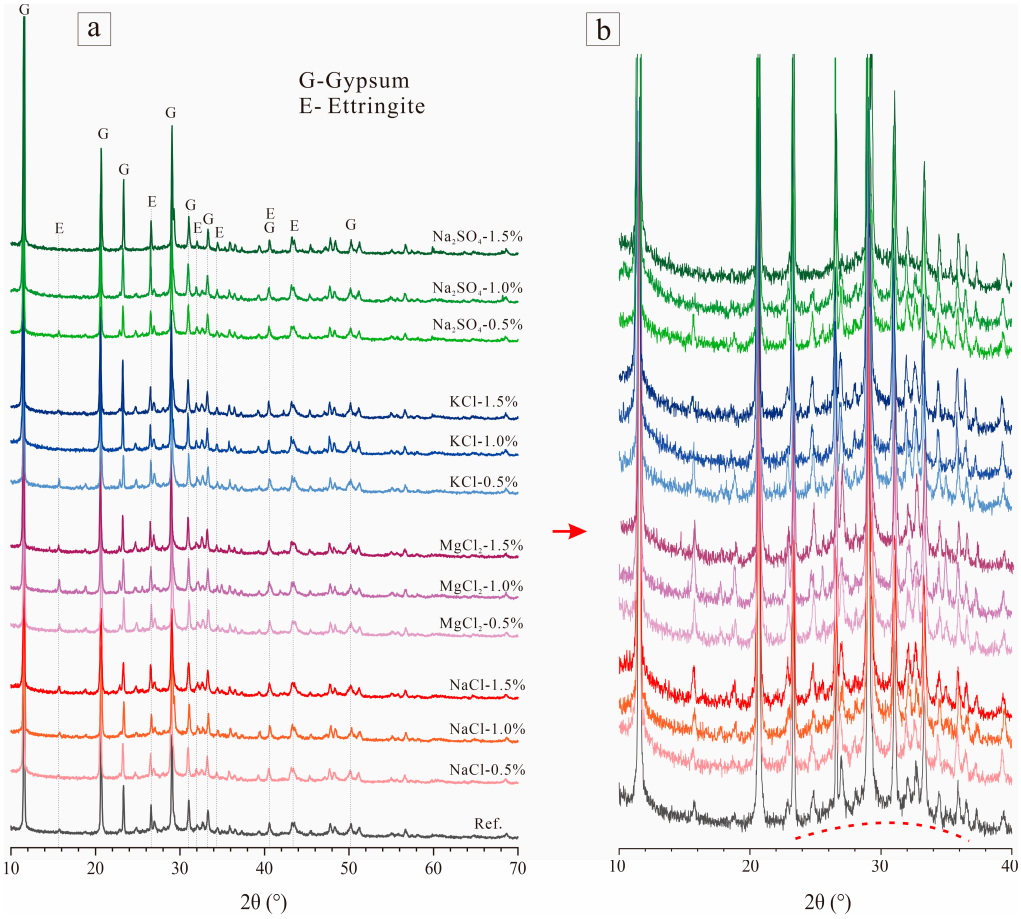


**Figure 11.** XRD pattern of EPSCs: (**a**) full scan spectra, (**b**) magnified view highlighting the 20–40° region.

It is noteworthy that the addition of different salts did not result in significant changes to the XRD pattern compared to the control group. The main hydration products remained dihydrate gypsum, ettringite, and C-(A)-S-H, which is likely attributed to the low concentration of salts. However, in the sample with 0.5% NaCl, the diffraction peak of the C-(A)-S-H gel was noticeably enhanced, aligning with the observed increase in the compressive and flexural strength of the EPSC. Furthermore, in the sample containing $Na_2SO_4$, the diffraction peak intensity of gypsum and ettringite increased significantly, indicating that $Na_2SO_4$ promotes the formation of these compounds. In the early stages of hydration in EPSC, the initial skeletal structure of the system is primarily formed by interlinked dihydrate gypsum crystals, which contribute to the strength of the early hardened matrix [17]. This observation corresponds closely with the substantial improvement in early compressive strength observed in EPSC with $Na_2SO_4$. While the mineral composition of all EPSC pastes remains similar, the addition of salts can significantly influence the compressive strength of EPSC by altering its microstructure.

### *3.5. SEM Images and EDX Results*

A detailed analysis of the hydration products of EPSC using SEM-EDX was performed. As shown in Figure 12a, the hydration products of EPSC without added salt primarily consist of gypsum, needle-shaped AFt, and flocculent C-(A)-S-H gel. These findings align closely with the results obtained through XRD analysis. A significant amount of hydration products was observed to form on the surface of gypsum, creating a strong bond with the EPSC matrix, which serves as the primary source of strength for the system. At higher magnifications (6000×), numerous AFt structures and C-(A)-S-H gel were seen to interweave tightly, forming a secondary skeleton structure that further enhances the overall strength of EPSC. This demonstrates that even when the PG content reaches 50 wt%, EPSC continues to exhibit excellent mechanical properties.

When comparing the microstructures of the three pastes at the same curing time (28 days), it was observed that the incorporation of $MgCl_2$ led to the formation of numerous pores within the matrix, resulting in a loose microstructure. Under high magnification (Figure 12d), many isolated particles were evident in the matrix, and the hydration products appeared to be significantly fewer than those in the control group. This reduction in hydration products corresponded to a notable decrease in compressive strength with the addition of 1% $MgCl_2$. Energy-dispersive X-ray (EDX) analysis of point #1 (Figure 12g) identified the presence of the elements O, S, Al, Si, and Ca, suggesting that the hydration products primarily consisted of C-(A)-S-H, gypsum, and AFt. In contrast, the EDX analysis of point #2 revealed the presence of Mg, indicating that a fraction of $Mg^{2+}$ ions had replaced $Ca^{2+}$ in the formation of C-(A)-S-H. Previous studies have highlighted that $Mg^{2+}$ tends to distribute unevenly within the matrix and may precipitate as $Mg(OH)_2$, $MgSO_4$, or $MgSiO_3$ (M-S-H) [20]. The substantial increase in overall porosity suggests that magnesium-based phases contribute only minimally to the system's strength.

Figure 12c,d depict the surface morphology of EPSC paste containing 1% KCl, which differs from the morphology observed with the addition of $MgCl_2$. However, the variation compared to the group without the salt addition is not significantly pronounced. Upon adding 1% KCl, a trace amount of K was detected in the matrix at point #3. EDX analysis at point #4 (refer to Figure 12g) reveals that the primary elements are Ca, S, and O, confirming that the hydration product is gypsum. The SEM image distinctly highlights the presence of gypsum, which is intricately integrated with C-(A)-S-H, resulting in a dense microstructure. Furthermore, Figure 12d demonstrates that the surface structure is densely packed, with a substantial amount of AFt wrapped and covered by a C-S-H gel layer on the surface.

Figure 13 displays the SEM images and EDX area scanning results for NaCl-1.0%. The findings show that the addition of 1% NaCl results in a relatively dense microstructure of EPSC, with minimal visible pores observed at a magnification of 500x. This corresponds to the material's high 28 days compressive strength. The EDX analysis confirms that the sample primarily comprises elements such as Ca, Si, O, Al, and S, aligning with the results of the XRD analysis. Furthermore, the incorporation of NaCl does not alter the types of hydration products, which remain predominantly gypsum, C-(A)-S-H, and AFt. The trace amounts of the Na element are primarily sourced from the added $Na_2SO_4$, which is dispersed uniformly throughout the sample. It is hypothesized that the sodium phase exists mainly in the form of N-(A)-S-H. Due to its lower reactivity compared to the calcium phase, only a small fraction of the sodium phase participates in the polymerization of N-(A)-S-H [37,45]. Additionally, the distribution of the elements Ca, Si, and Al is noticeably more compact.

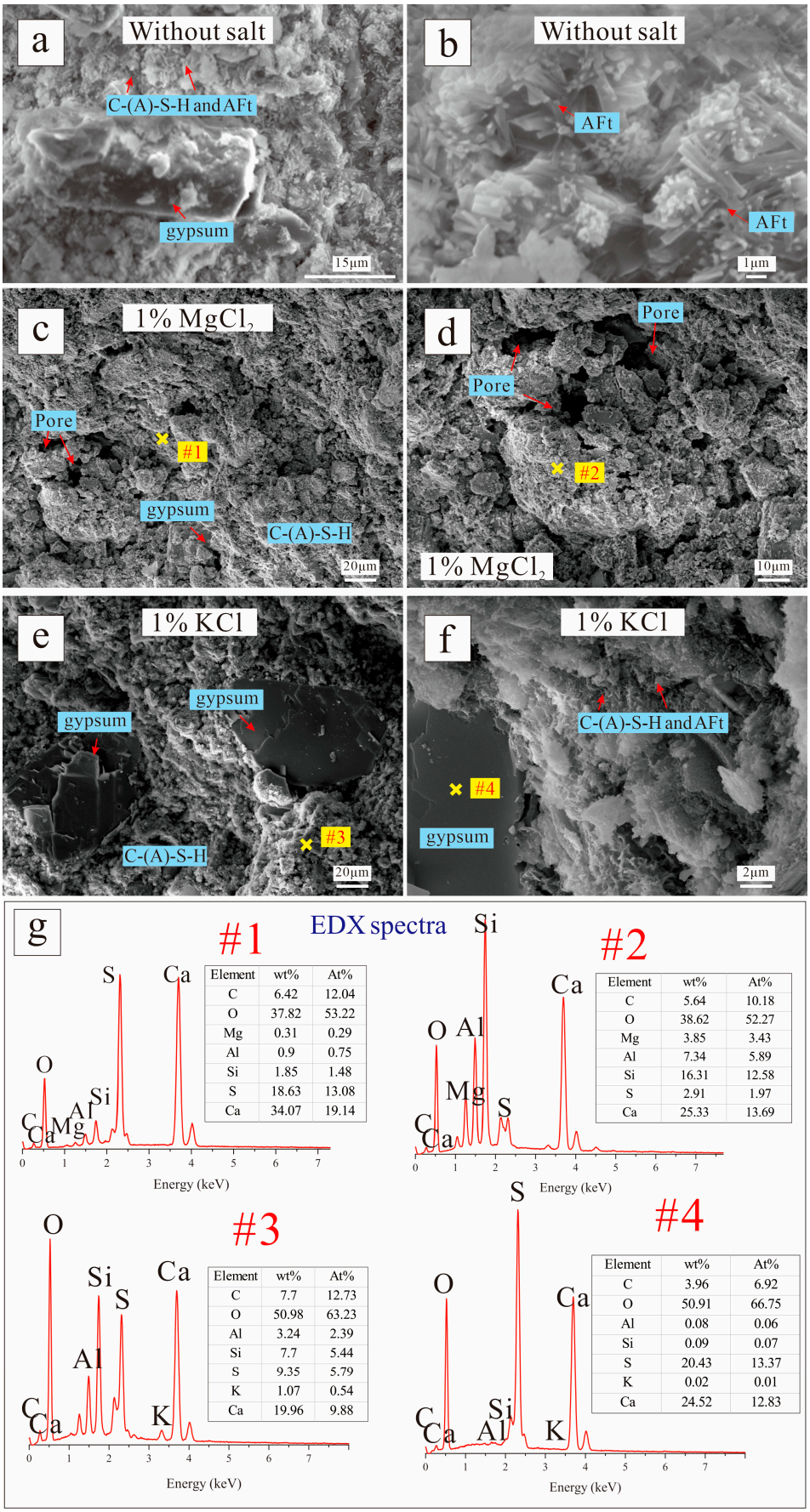


**Figure 12.** SEM images and EDX result of EPSCs (28 days): (**a**,**b**) without salt; (**c**,**d**) 1% $MgCl_2$; (**e**,**f**) KCl; and (**g**) EDX spectra.

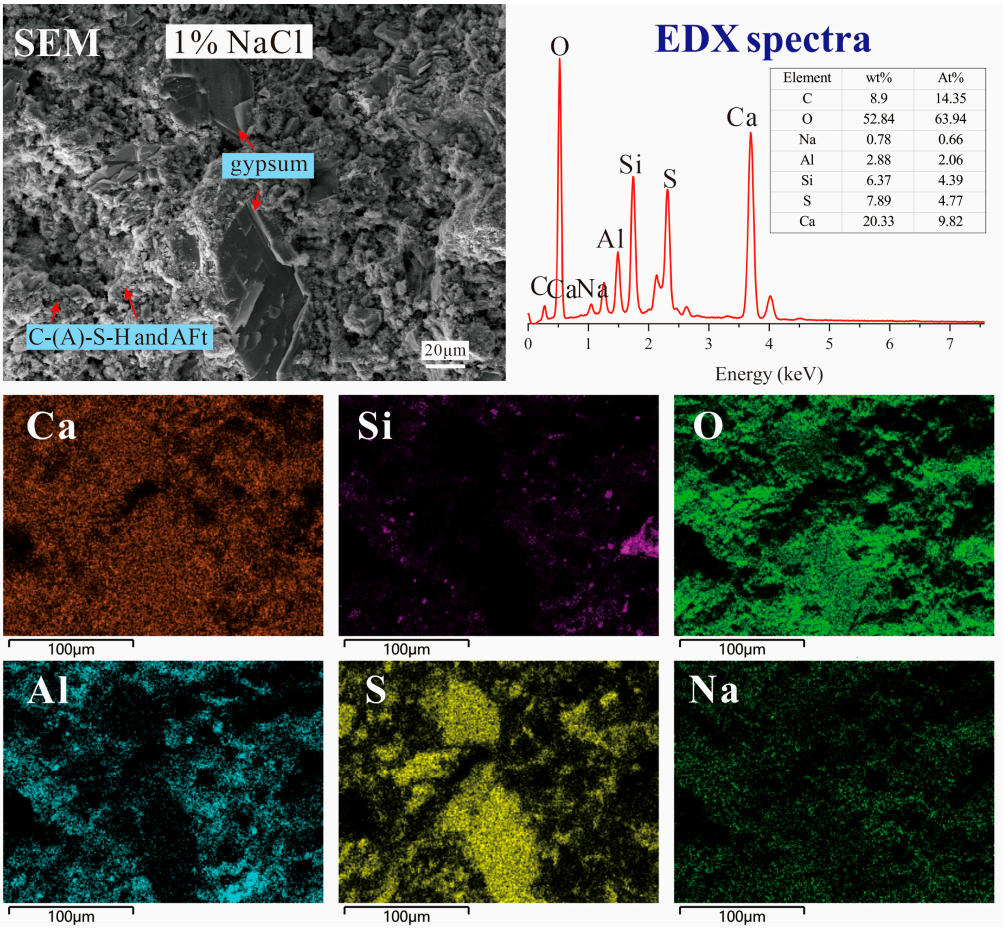


**Figure 13.** SEM images and EDX elemental mapping of NaCl-1.0% after 28 days.

The formation of AFt is closely influenced by the concentrations of $Ca^{2+}$, $Al^{3+}$, and $SO_4^{2-}$ in the system, as well as the pH of the liquid phase. During the hydration process of EPSC, the elevated content of PG ensures that gypsum remains in excess throughout. Consequently, the primary factors governing the AFt content are the $Ca(OH)_2$ produced by the hydration of ordinary Portland cement and the $Al^{3+}$ released during the hydration of GGBFS [18,46]. The alkalinity of the liquid phase plays a critical role in determining the hydrolysis rate of GGBFS. The introduction of $Na_2SO_4$ directly impacts system alkalinity, subsequently affecting the hydration behavior of raw materials and promoting AFt formation. As illustrated in Figure 14, the degree of hydration decreased following the addition of $Na_2SO_4$. Although significant AFt formation was observed, pores remain visible in the corresponding SEM images. Previous research has indicated that while the addition of $Na_2SO_4$ can support early-stage microstructural development, it inhibits the hydration of GGBFS by altering the pathway of microstructural evolution [42]. From an engineering perspective, this phenomenon may pose durability risks. Porosity may enable corrosive ions (e.g., $Cl^-$, $SO_4^{2-}$) to penetrate, exacerbating material degradation in saline environments such as marine infrastructure or saline-soil foundations. Additionally, uncontrolled AFt formation could generate delayed expansion stresses, jeopardizing long-term dimensional stability. Thus, precise $Na_2SO_4$ dosage optimization is essential to reconcile early-stage performance enhancements with lifecycle reliability in EPSC implementations.

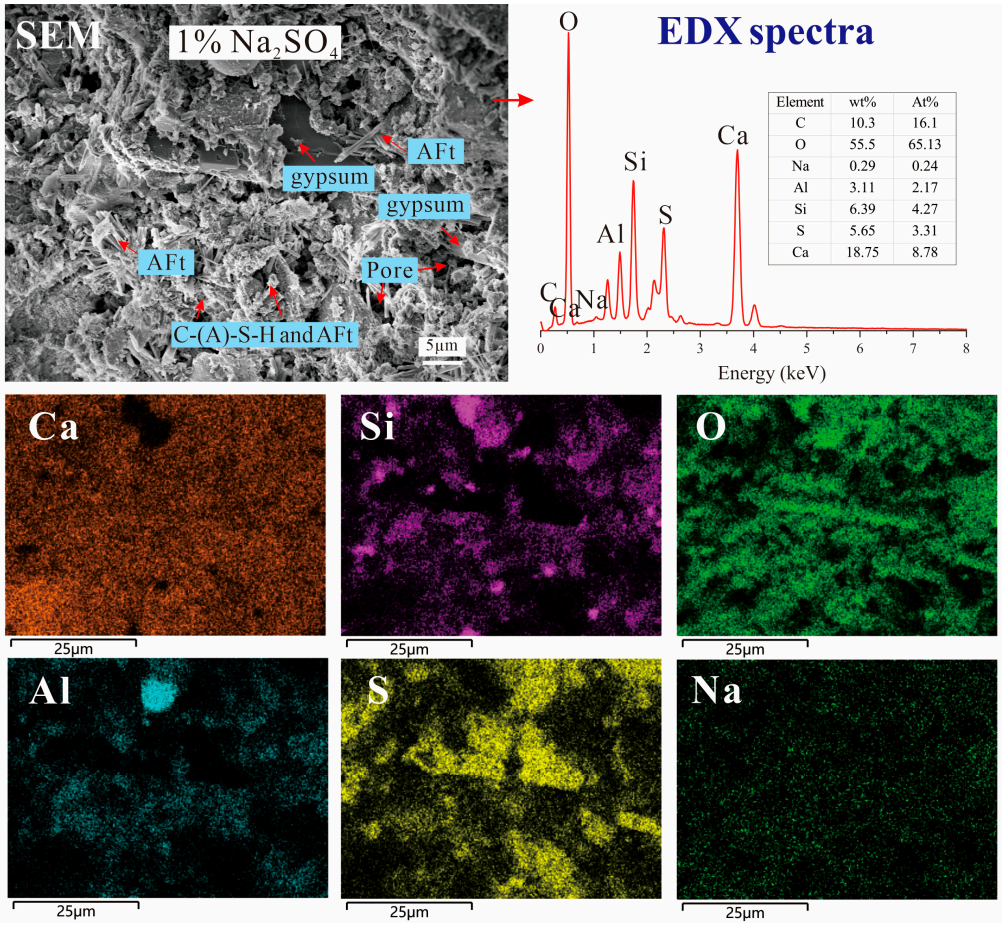


**Figure 14.** SEM images and EDX elemental mapping of $Na_2SO_4$-1.0% after 28 days.

## 4. Conclusions

This study systematically investigates the effects of four common salts (NaCl, $MgCl_2$, KCl, and $Na_2SO_4$) on the performance of EPSC. Comprehensive analyses were conducted on rheological behavior, mechanical properties, hydration products, and microstructure. The key findings are summarized as follows:

(1) EPSC exhibits low initial yield stress and plastic viscosity, attributed to the weak gelling capacity of PG and slow GGBFS hydration. However, both parameters increase significantly over time. All pastes follow the modified Bingham model and display consistent shear-thinning behavior.

(2) $Na^+$, $Cl^-$, and $SO_4^{2-}$ promote hydration and flocculent structure formation, enhancing yield stress and plastic viscosity. In contrast, $Mg^{2+}$ and $K^+$ retard or alter hydration pathways. Notably, $Mg^{2+}$ temporarily increases plastic viscosity early on due to $Mg(OH)_2$ formation.

(3) Salt content exhibits a threshold effect. $Na_2SO_4$ and NaCl improve mechanical properties at 0.5–1.0%, but higher concentrations (>1%) are detrimental. With 0.5% NaCl, EPSC achieves a 28-day compressive strength of 51.06 MPa (9.5% higher than the control). Conversely, $MgCl_2$ reduces strength due to low-strength $Mg(OH)_2$ from $Mg^{2+}$ substitution.

(4) $Na_2SO_4$ boosts early strength (47.9% increase at 7 days) by raising pH and forming dispersible $CaSO_4$, accelerating ettringite and C-(A)-S-H gel formation. However, excessive ettringite may compromise strength, owing to EPSC's inherent high $SO_4^{2-}$ content.

(5) XRD and SEM-EDX confirm that salts do not change primary hydration products (ettringite, gypsum, C-(A)-S-H) but modify microstructure via ion migration and crystal-

lization. NaCl improves pore structure by forming Friedel's salt, while $Na_2SO_4$ promotes early ettringite nucleation.

(6) $Na_2SO_4$ uniquely elevates the flexural-to-compressive strength ratio (0.19–0.24 vs. 0.18–0.20 for other salts), as needle-like ettringite enhances flexural resistance.

This study reveals the effects of inorganic salts on the rheological properties, mechanical properties, and microstructure of EPSC, providing new insights into the role of salts in the preparation process of EPSC and facilitating the reuse and recycling of PG.

**Author Contributions:** Conceptualization, W.L., Y.F. and J.X.; Data curation, Y.X. and J.M.; Formal analysis, Z.X.; Funding acquisition, J.X.; Investigation, Z.C., Z.X., Y.X. and C.W.; Methodology, Z.C.; Project administration, Y.F.; Resources, Y.X.; Software, C.W. and J.M.; Validation, C.W.; Writing—original draft, Z.C., Z.X. and Y.F.; Writing—review and editing, W.L. and Y.F. All authors have read and agreed to the published version of the manuscript.

**Funding:** The authors gratefully acknowledge the financial support provided by the Science and Technology Planning Project of Guangdong Province (Grant No. 2022A0505050077), the National Natural Science Foundation of China (Grant No. 12372180), and the Guangdong Basic and Applied Basic Research Foundation (Grant No. 2023A1515012180).

**Data Availability Statement:** The original contributions presented in the study are included in the article, further inquiries can be directed to the corresponding author.

**Conflicts of Interest:** Authors Zhe Chen, Zixin Xue, Yong Xia, Chunli Wu and Junming Mai were employed by the company Guangdong Building Materials Institute Co., Ltd. The remaining authors declare that the research was conducted in the absence of any commercial or financial relationships that could be construed as a potential conflict of interest.

## Abbreviations

| | |
|---|---|
| EPSC | excess-sulfate phosphogypsum slag cement |
| PG | phosphogypsum |
| GGBFS | ground granulated blast furnace slag |
| AFt | ettringite |

## References

1. Olivier, J.G.; Peters, J.A.; Janssens-Maenhout, G. *Trends in Global $CO_2$ Emissions: 2012 Report*; U.S. Department of Energy: Washington, DC, USA, 2012.
2. Jin, Z.; Zhao, X.; Du, Y.; Yang, S.; Wang, D.; Zhao, T.; Bai, Y. Comprehensive properties of passive film formed in simulated pore solution of alkali-activated concrete. *Constr. Build. Mater.* **2022**, *319*, 126142. [CrossRef]
3. Nandhini, K.; Karthikeyan, J. Sustainable and greener concrete production by utilizing waste eggshell powder as cementitious material–A review. *Constr. Build. Mater.* **2022**, *335*, 127482. [CrossRef]
4. Feng, Y.; Zhang, B.; Xie, J.; Xue, Z.; Huang, K.; Tan, J. Effects of recycled sand and nanomaterials on ultra-high performance concrete: Workability, compressive strength and microstructure. *Constr. Build. Mater.* **2023**, *378*, 131180. [CrossRef]
5. Li, L.; Xie, J.; Zhang, B.; Feng, Y.; Yang, J. A state-of-the-art review on the setting behaviours of ground granulated blast furnace slag-and metakaolin-based alkali-activated materials. *Constr. Build. Mater.* **2023**, *368*, 130389. [CrossRef]
6. Gu, K.; Chen, B.; Pan, Y. Utilization of untreated-phosphogypsum as filling and binding material in preparing grouting materials. *Constr. Build. Mater.* **2020**, *265*, 120749. [CrossRef]
7. Al-Masri, M.; Amin, Y.; Ibrahim, S.; Al-Bich, F. Distribution of some trace metals in Syrian phosphogypsum. *Appl. Geochem.* **2004**, *19*, 747–753. [CrossRef]
8. Rashad, A.M. Phosphogypsum as a construction material. *J. Clean. Prod.* **2017**, *166*, 732–743. [CrossRef]
9. Hentati, O.; Abrantes, N.; Caetano, A.L.; Bouguerra, S.; Goncalves, F.; Römbke, J.; Pereira, R. Phosphogypsum as a soil fertilizer: Ecotoxicity of amended soil and elutriates to bacteria, invertebrates, algae and plants. *J. Hazard. Mater.* **2015**, *294*, 80–89. [CrossRef]
10. Shen, W.; Gan, G.; Dong, R.; Chen, H.; Tan, Y.; Zhou, M. Utilization of solidified phosphogypsum as Portland cement retarder. *J. Mater. Cycles Waste Manag.* **2012**, *14*, 228–233. [CrossRef]
11. Wang, Y.; Huo, H.; Chen, B.; Cui, Q. Development and optimization of phosphogypsum-based geopolymer cement. *Constr. Build. Mater.* **2023**, *369*, 130577. [CrossRef]

12. Wang, Y.; Chen, B.; Liu, N.; Jiang, Z. Utilization of waste phosphogypsum in high-strength geopolymer concrete: Performance optimization and mechanistic exploration. *J. Build. Eng.* **2024**, *98*, 111253. [CrossRef]
13. Feng, Y.; Xue, Z.; Zhong, H.; Zhang, B.; Yang, J.; Xie, J. Improving geopolymer concrete performance with hazardous solid waste phosphogypsum. *J. Build. Eng.* **2024**, *95*, 110333. [CrossRef]
14. Feng, Y.; Xue, Z.; Zhang, B.; Xie, J.; Chen, C.; Tan, J.; Zhao, C. Effects of phosphogypsum substitution on the performance of ground granulated blast furnace slag/fly ash-based alkali-activated binders. *J. Build. Eng.* **2023**, *70*, 106387. [CrossRef]
15. Li, H.; Xu, F.; Li, B.; Sun, T.; Huang, X.; Zhu, J.; Peng, C.; Lin, J.; Chen, Z. Investigation on mechanical properties of excess-sulfate phosphogypsum slag cement: From experiments to molecular dynamics simulation. *Constr. Build. Mater.* **2022**, *315*, 125685. [CrossRef]
16. Ouyang, G.; Li, Z.; Sun, T.; Ye, Z.; Deng, Y.; Li, W. Greener phosphogypsum-based all-solid-waste cementitious binder with steel slag activation: Hydration, mechanical properties and durability. *J. Clean. Prod.* **2024**, *443*, 140996. [CrossRef]
17. Tao, L.; Deng, F.; Xu, K.; Dong, X.; Xu, D.; Liao, Y.; Tang, S. Effect of calcium sulfoaluminate cement on the hydration process and water resistance of phosphogypsum slag cement. *J. Mater. Res. Technol.* **2024**, *33*, 5375–5383. [CrossRef]
18. Xu, J.; Xu, F.; Jiang, Y.; Jiao, Y.; Sun, T.; Yang, F.; Wu, Y.; Chen, S.; Liu, Y.; Zhu, J.; et al. Mechanical properties and soluble phosphorus solidification mechanism of a novel high amount phosphogypsum-based mortar. *Constr. Build. Mater.* **2023**, *394*, 132176. [CrossRef]
19. Zhang, J.; Hu, C.; Shen, D.; Feng, Y.; Han, G.; An, X. Setting Time Optimization of Excessive-Sulfate Phosphogypsum Slag Cement for Self-Compacting Concrete Based on a Paste Rheological Threshold Theory. *J. Mater. Civ. Eng.* **2024**, *36*, 04024285. [CrossRef]
20. Zhang, B.; Huang, D.; Li, L.; Lin, M.; Liu, Y.; Fang, W.; Lu, J.; Liu, F.; Li, Y.; Liu, Y.; et al. Effect of magnesium salt contamination on the microstructures and properties of metakaolinite-based geopolymer: The role of $MgCl_2$ and $MgSO_4$. *J. Mater. Res. Technol.* **2022**, *20*, 4500–4514. [CrossRef]
21. Liu, W.; Zhao, J.; Feng, Y.; Zhang, B.; Xie, J. Seawater-mixed alkali-activated materials: A state-of-the-art review. *J. Mater. Sci.* **2025**, *60*, 2169–2198. [CrossRef]
22. Chen, J.; Jia, J.; Zhu, M. Development of admixtures on seawater sea sand concrete: A critical review on Concrete hardening, chloride ion penetration and steel corrosion. *Constr. Build. Mater.* **2024**, *411*, 134219. [CrossRef]
23. Zhang, T.; Tan, H.; Ni, J.; Ma, B.; Liu, X.; Chen, P.; Shi, T. Effect of barium ion on the stability and chloride ion binding of ettringite. *J. Build. Eng.* **2023**, *79*, 107803. [CrossRef]
24. Cai, Y.; Tao, Y.; Xuan, D.; Sun, Y.; Poon, C.S. Effect of seawater on the morphology, structure, and properties of synthetic ettringite. *Cem. Concr. Res.* **2023**, *163*, 107034. [CrossRef]
25. Ting, M.Z.Y.; Yi, Y. Durability of cementitious materials in seawater environment: A review on chemical interactions, hardened-state properties and environmental factors. *Constr. Build. Mater.* **2023**, *367*, 130224. [CrossRef]
26. Marks, V.J.; Dubberke, W.G. A different perspective for investigation of portland cement concrete pavement deterioration. *Transp. Res. Rec.* **1996**, *1525*, 91–96. [CrossRef]
27. Song, S.; Sohn, D.; Jennings, H.; Mason, T. Hydration of alkali-activated ground granulated blast furnace slag. *J. Mater. Sci.* **2000**, *35*, 249–257. [CrossRef]
28. Rashad, A.; Bai, Y.; Basheer, P.; Milestone, N.; Collier, N. Hydration and properties of sodium sulfate activated slag. *Cem. Concr. Compos.* **2013**, *37*, 20–29. [CrossRef]
29. Al-kroom, H.; Arif, M.A.; Saleh, A.A.; Shalaby, H.M.; Abd Elrahman, M.; Abdel-Gawwad, H.A. The role of nano magnesia in accelerating the early hydration rate of sodium sulfate activated slag. *Constr. Build. Mater.* **2023**, *373*, 130863. [CrossRef]
30. Zhang, B.; Feng, Y.; Xie, J.; Dai, J.; Chen, W.; Xue, Z.; Li, L.; Li, Y.; Li, J. Effects of pretreated recycled powder substitution on mechanical properties and microstructures of alkali-activated cement. *Constr. Build. Mater.* **2023**, *406*, 133360. [CrossRef]
31. Wang, J.; Mu, M.; Liu, Y. Recycled cement. *Constr. Build. Mater.* **2018**, *190*, 1124–1132. [CrossRef]
32. Sun, T.; Li, W.; Xu, F.; Yu, Z.; Wang, Z.; Ouyang, G.; Xu, D. A new eco-friendly concrete made of high content phosphogypsum based aggregates and binder: Mechanical properties and environmental benefits. *J. Clean. Prod.* **2023**, *400*, 136555. [CrossRef]
33. *GB/T 7714-2015*; Test Method of Cement Mortar Strength (ISO Method). Standards Press of China: Beijing, China, 2015.
34. Zhao, Y.; Qiu, J.; Zhang, S.; Guo, Z.; Ma, Z.; Sun, X.; Xing, J. Effect of sodium sulfate on the hydration and mechanical properties of lime-slag based eco-friendly binders. *Constr. Build. Mater.* **2020**, *250*, 118603. [CrossRef]
35. Mahmoodzadeh, F.; Chidiac, S. Rheological models for predicting plastic viscosity and yield stress of fresh concrete. *Cem. Concr. Res.* **2013**, *49*, 1–9. [CrossRef]
36. Chen, Z.; Zhao, G.; Chen, B.; Chen, S.; Li, J.; Nong, Y. Influence of flocculation structure on time-dependent fluidity and rheological property of cement paste: Analytical models based on fractal theory. *Constr. Build. Mater.* **2024**, *455*, 139137. [CrossRef]
37. Xiang, J.; Qiu, J.; Zhao, Y.; Zheng, P.; Peng, H.; Fei, X. Rheology, mechanical properties, and hydration of synergistically activated coal gasification slag with three typical solid wastes. *Cem. Concr. Compos.* **2024**, *147*, 105418. [CrossRef]
38. Shi, Z.; Shi, C.; Liu, H.; Li, P. Effects of triisopropanol amine, sodium chloride and limestone on the compressive strength and hydration of Portland cement. *Constr. Build. Mater.* **2016**, *125*, 210–218. [CrossRef]

39. Rocha, C.A.A.; Cordeiro, G.C.; Toledo Filho, R.D. Use of thermal analysis to determine the hydration products of oil well cement pastes containing NaCl and KCl. *J. Therm. Anal. Calorim.* **2015**, *122*, 1279–1288. [CrossRef]
40. Pang, X.; Boul, P.; Jimenez, W.C. Isothermal calorimetry study of the effect of chloride accelerators on the hydration kinetics of oil well cement. *Constr. Build. Mater.* **2015**, *77*, 260–269. [CrossRef]
41. Puertas, F.; Fernández-Jiménez, A.; Blanco-Varela, M. Pore solution in alkali-activated slag cement pastes. Relation to the composition and structure of calcium silicate hydrate. *Cem. Concr. Res.* **2004**, *34*, 139–148. [CrossRef]
42. Fu, J.; Bligh, M.W.; Shikhov, I.; Jones, A.M.; Holt, C.; Keyte, L.M.; Moghaddam, F.; Arns, C.H.; Foster, S.J.; Waite, T.D. A microstructural investigation of a Na2SO4 activated cement-slag blend. *Cem. Concr. Res.* **2021**, *150*, 106609. [CrossRef]
43. Nguyen, H.; Adesanya, E.; Ohenoja, K.; Kriskova, L.; Pontikes, Y.; Kinnunen, P.; Illikainen, M. Byproduct-based ettringite binder–a synergy between ladle slag and gypsum. *Constr. Build. Mater.* **2019**, *197*, 143–151. [CrossRef]
44. Shi, C.; Tang, X.; Li, Y. Thermal activation of phosphorus slag. *Cement* **1991**, *88*, 219.
45. Xue, J.; Liu, S.; Ma, X.; Teng, Y.; Guan, X. Effect of different gypsum dosage on the chloride binding properties of C4AF hydrated paste. *Constr. Build. Mater.* **2022**, *315*, 125562. [CrossRef]
46. Goetz-Neunhoeffer, F.; Neubauer, J.; Schwesig, P. Mineralogical characteristics of Ettringites synthesized from solutions and suspensions. *Cem. Concr. Res.* **2006**, *36*, 65–70. [CrossRef]


**Disclaimer/Publisher's Note:** The statements, opinions and data contained in all publications are solely those of the individual author(s) and contributor(s) and not of MDPI and/or the editor(s). MDPI and/or the editor(s) disclaim responsibility for any injury to people or property resulting from any ideas, methods, instructions or products referred to in the content.